

Article

Indications that Amorphous Calcium Carbonates Occur in Pathological Mineralisation—A Urinary Stone from a Guinea Pig

Denis Gebauer ^{1,*} , Kjell Jansson ², Mikael Oliveberg ³ and Niklas Hedin ^{2,*} 

¹ Department of Chemistry, Physical Chemistry, University of Konstanz, Universitätsstraße 10, D-78464 Konstanz, Germany

² Department of Materials and Environmental Chemistry, Arrhenius Laboratory, Stockholm University, SE-106 91 Stockholm, Sweden; kjell.jansson@mmk.su.se

³ Department of Biochemistry and Biophysics, Arrhenius Laboratories of Natural Sciences, Stockholm University, S-106 91 Stockholm, Sweden; mikael.oliveberg@dbb.su.se

* Correspondence: denis.gebauer@uni-konstanz.de (D.G.); niklas.hedin@mmk.su.se (N.H.); Tel.: +49-7531-88-2169 (D.G.); +46-8-16-24-17 (N.H.)

Received: 29 January 2018; Accepted: 24 February 2018; Published: 27 February 2018

Abstract: Calcium carbonate is an abundant biomineral that is of great importance in industrial or geological contexts. In recent years, many studies of the precipitation of CaCO₃ have shown that amorphous precursors and intermediates are widespread in the biomineralization processes and can also be exploited in bio-inspired materials chemistry. In this work, the thorough investigation of a urinary stone of a guinea pig suggests that amorphous calcium carbonate (ACC) can play a role in pathological mineralization. Importantly, certain analytical techniques that are often applied in the corresponding analyses are sensitive only to crystalline CaCO₃ and can misleadingly exclude the relevance of calcium carbonate during the formation of urinary stones. Our analyses suggest that ACC is the major constituent of the particular stone studied, which possibly precipitated on struvite nuclei. Minor amounts of urea, other stable inorganics, and minor organic inclusions are observed as well.

Keywords: amorphous calcium carbonate; urinary stones; guinea pig; pathological mineralization; struvite

1. Introduction

Calcium carbonate is the most abundant biomineral and is the inorganic constituent of mussel shells, the carapace of crayfish and lobsters, the exoskeleton of corals, and an important biomineral in many more organisms [1]. Moreover, it is of major industrial (building industries), economic (scaling and incrustation), and ecological (climate) importance [2]. Studies of biomineralization serve as an inspiration for material scientists, as biogenic composites show outstanding performance in terms of material properties [3], which is rare in artificial counterparts [4–6]. The level of control over the crystallization processes in organisms is very high, but the underlying molecular mechanisms are still not understood in detail [7]. In general, it is accepted that organisms use amorphous intermediates during the biomineralization of calcium carbonates [8–10]. These intermediates appear to be crucial to the generation of complex hierarchical structures of many biomineralized exoskeletons [8,9].

Controlling crystallization is, however, not only linked to the generation of mineral-based hybrid materials but also to the inhibition of the unwanted precipitation of minerals. In organisms, pathological mineralization can lead to severe issues in soft tissues, the formation of mineral stones in bodily fluids, or the uncontrolled growth of hard tissues [11–14]. Organisms employ specific

proteins to inhibit unwanted mineralization, which range from the blood-protein family of fetuins [11] to statherin (saliva) [15]. However, when it comes to pathological mineralization in mammals, the formation of less soluble calcium phosphates and oxalates is often more critical than uncontrolled precipitation of CaCO_3 [11,16,17]. An example of functionally formed calcium carbonate stones is the gastroliths of lobsters [8,10,18]. They serve as a calcium reservoir regularly needed upon molting, as the carapace cannot grow with the animal. Gastroliths are mostly constituted of amorphous calcium carbonate (ACC) [19], due to its higher solubility and better bioavailability as compared to crystalline calcium carbonates. One example of pathologically formed calcium carbonate is the urinary stones of guinea pigs. They typically contain large amounts of calcium carbonate, often up to 100%, and mostly constitute calcite, magnesian calcite, or monohydrocalcite [20,21]. The occurrence of ACC in such stones has not been reported so far, to the best of our knowledge.

In fact, the general relevance of ACC in the formation calcium carbonates is currently under debate [22,23]. From the point of view of classical nucleation theory, ACC is only accessible beyond a certain level of supersaturation, and is thus often assumed, arbitrarily, to not occur in many settings that are nominally undersaturated with respect to macroscopic phases of ACC [24]. However, there are indications from computer simulations of ACC being the thermodynamically stable form of CaCO_3 at small particle sizes ($< \sim 4$ nm) [25]. Indeed, alternative views on the mechanism of phase separation, e.g., according to the so-called pre-nucleation cluster pathway, suggest that ACC would always form first, transiently [7], while recent in-situ electron microscopy studies suggest that crystalline calcium carbonate can form in solution via direct pathways [23]. The role of the electron beam in such experiments remains unclear, especially when it comes to the induction of crystallisation in amorphous intermediates [26].

In any case, the fundamental question regarding the occurrence of ACC is of ultimate relevance for pathological mineralisation as well. On the one hand, ACC can be overseen when techniques are employed that are only sensitive towards the detection of crystalline species, such as X-ray diffraction (XRD) [21]. This approach can lead to misinterpretations of stone compositions and bring about erroneous assessments of the consequences of dietary conditions. We do note that the occurrence of amorphous carbonated calcium phosphate (ACCP) in pathological mineralization is thoroughly established [27]; however, also, the role of ACC in pathological mineralisation could be a more widespread phenomenon. Strategies to inhibit nucleation and crystallisation, within the notions of alternative pathways to particle formation [7,28,29], may potentially allow for the development of new medical treatments, perhaps even beyond the calcium-carbonate-rich urinary stones in guinea pigs.

This study has been conducted on a particular stone of an individual guinea pig. It has a mixed inorganic composition of calcium carbonates and magnesium ammonium phosphate hexahydrate (struvite), indicating that the stone had formed upon urinary tract infection [30,31]. A global discussion of a combination of results indicates that a significant fraction of the calcium carbonate is amorphous. It appears as amorphous precursors, and intermediates could play a key role also in the pathological mineralisation of such stones.

2. Materials and Methods

Urinary stones. No animals were harmed in the course of this study; the urinary stone specimen was provided by Mia Winge of a non-profit organization for helping guinea pigs: <http://www.marsvinshjalpen.se>.

Scanning electron microscopy (SEM) and energy-dispersive X-ray spectroscopy (EDS). A urinary stone was cut through the centre utilising a blade saw, and gently polished under dry conditions, first using SiC paper (4000 mesh) and then diamond paper (1 micrometre). After polishing, the remaining loose abrasive material was blown away by a gentle air stream. This polished stone was imaged utilising the detector for back-scattered electrons in a SEM. To that end, a TM 3000 table scanning electron microscope (Hitachi, Tokio, Japan) was used with an accelerating voltage of 15 kV. EDS mapping was performed using a SDD detector (Quantax 70, Bruker, Billerica, MA, USA), and

the spectra were analysed for three particular areas. This analysis is self-calibrating and relatively insensitive to local sample tilts and surface conditions.

Fourier transform infrared (FT-IR) spectroscopy. FT-IR spectra were recorded on a finely ground powder of a urinary stone with a 670-IR FT-IR spectrometer (Varian, Palo Alto, CA, USA) and its diamond-based attenuated total reflectance device (Golden Gate™, Specac, Orpington, UK) within a spectral range of 390–4000 cm^{-1} and a spectral resolution of 2 cm^{-1} . The room temperature detector of the spectrometer was used.

Thermal gravimetric analysis (TGA). TGA of a piece of the urinary stone was conducted on a TGA 7 analyser (Perkin Elmer, Waltham, MA, USA) by heating the sample from 25 to 900 °C at a rate of 2 °C/min under a flow of dry artificial air mixture.

X-ray powder diffraction (XRD). Diffractograms were recorded on a X'Pert Pro diffractometer (PANalytical, Almelo, The Netherlands) using $\text{Cu K}\alpha_1$ ($\lambda = 1.5406 \text{ \AA}$) radiation and a PIXel detector. The diffractograms were acquired for $20^\circ < 2\theta < 60^\circ$ using a scanning speed of 0.04° s^{-1} (acquisition time of ~17 minutes per diffractogram). Pieces of a urinary stone were finely ground, dispersed in isopropanol, and subsequently spread on silicon plates, uniformly.

3. Results and Discussion

The SEM images in Figure 1 of a gently polished stone exemplify successive regions of dense and porous areas that appear to have grown in rings. The dense rings alternate with loose and porous regions, similar to the concentric rings that Peng et al. observed by optical microscopy of a stone composed of calcium carbonate, magnesium ammonium phosphate hexahydrate (struvite), and calcium phosphate [32]. The infrared spectrum recorded on the stone displays distinct bands that can be assigned to the different vibrational modes of CO_3^{2-} and PO_4^{3-} ions (Figure 2). In addition, bands typical for CH_3 , CH_2 , and NH chemical groups are observed, as one would expect from the inclusion of proteins and other biomolecules. The assignments of bands in the fingerprint region ($<1000 \text{ cm}^{-1}$) are consistent with the crystalline inorganic polymorphs as established by XRD data (see below) and can be assigned to phosphates and carbonates.

The band at 995 cm^{-1} is due to the anti-symmetric stretching mode (ν_3) of the phosphate ion, which is triply degenerate for free phosphates. It has earlier been reported to occur at 1006 cm^{-1} in magnesium ammonium phosphate hexahydrate (struvite) [33]. There is also a good match of the band frequency for the in-plane bending mode (ν_4) of the phosphate group (569 cm^{-1}), which has been reported to occur at 571 cm^{-1} in struvite [33]. The minor variances between the band positions and those in literature reports can be rationalized by the coupling with librational modes of water, which occur in this spectral region, as well as additional bands from calcium carbonate and organic compounds. The ν_3 band of the carbonate ion is located at 1402 cm^{-1} , whereas the band position and band width are rather inconclusive when it comes to discriminating in between ACC (split band 1392/1462 cm^{-1}) and calcite (1392 cm^{-1}) [34]. The broad band features a shoulder (~1469 cm^{-1}) that could relate to the split band that is normally observed for ACC and could include contributions from amide bands of proteins present in stone. The band for the out-of-plane bending mode (ν_2) at 872 cm^{-1} cannot be used directly to discriminate ACC from crystalline forms of CaCO_3 either, because its position varies for different types of ACC [35–40]. However, in this case, the band position agrees with literature reports on calcite [34]. Typically, the ν_4 bands of the carbonate ion are used to discriminate between ACC and different crystalline forms. These bands are sharp, although they are rather weak for calcite (713 cm^{-1}), vaterite (745 cm^{-1}), and aragonite (713/700 cm^{-1} split band) [41], and very weak and split for ACC (694/723 cm^{-1}) [34]. Actually, the ν_4 split bands of ACC are often not observable, since they are superimposed by a broad band that arises from the librational modes of (structural) water molecules [34]. In case of the urinary stone of the guinea pig, broad bands are located at 758/715 cm^{-1} with a minor shoulder at 702 cm^{-1} . The carbonate bands in the fingerprint region cannot directly be used to identify the very specific distribution of polymorphs of calcium carbonate present in the urinary stone of the guinea pig. Although some spectral features of calcite are observed,

the vibrational modes of the carbonates are much broader than what is typical for calcite, which is indicative of substantial structural disorder that may arise from ACC and/or disordered Mg-calcite. Since the spectral region for the carbonate ν_2 and ν_4 bands is superimposed by contributions from the phosphate bands and bands that arise from organic constituents, the ν_2/ν_4 -intensity ratio for the carbonate ions [42] cannot be unambiguously used to confirm the presence of ACC.

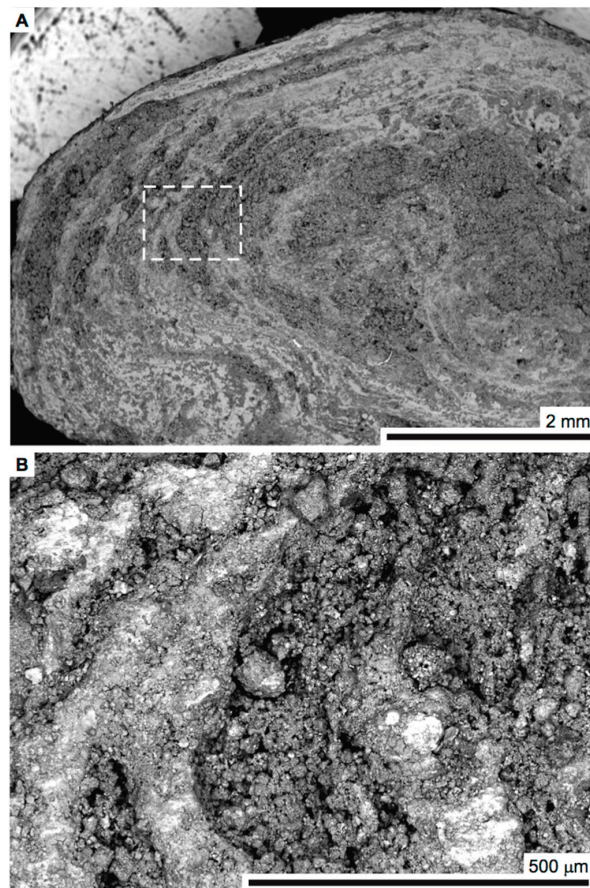


Figure 1. Scanning electron micrographs of a urinary stone from a guinea pig. The cross-section of the stone was polished, and images were recorded from backscattered electrons. (A) Overview and (B) magnified view of the dashed area indicated in (A).

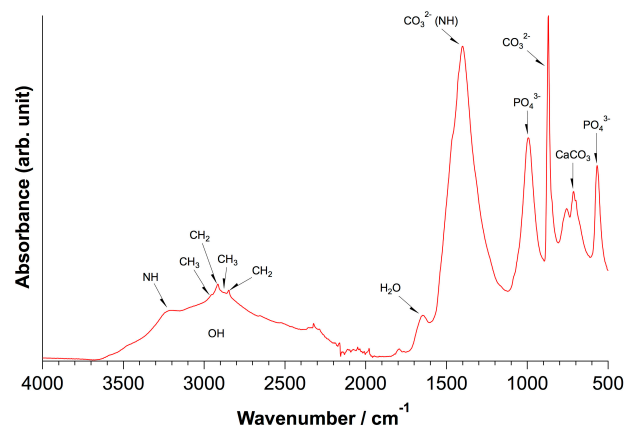


Figure 2. Fourier transform infrared spectrum of the powdered urinary stone.

XRD has often been used to identify and quantify the amounts of crystalline polymorphs in urinary stones of guinea pigs and other mammals [21]. The XRD diffractogram shown in Figure 3 indicates that struvite is present in the urinary stone studied here, alongside a poorly crystalline calcium carbonate phase, which is consistent with the IR analysis above; however, the XRD data cannot be unambiguously evaluated toward the amount of crystalline calcium carbonate owing to the unusual broad reflections and considerable noise level (see Figure 3, and further discussions below). Struvite has been observed in urinary stones of mammals in general [43]. The diffractogram (Figure 3) is a convolution of mainly two characteristic patterns of reflections, one set of reflections with narrow peak widths from struvite and one set with broad reflections that may be assigned to (Mg-)calcite.

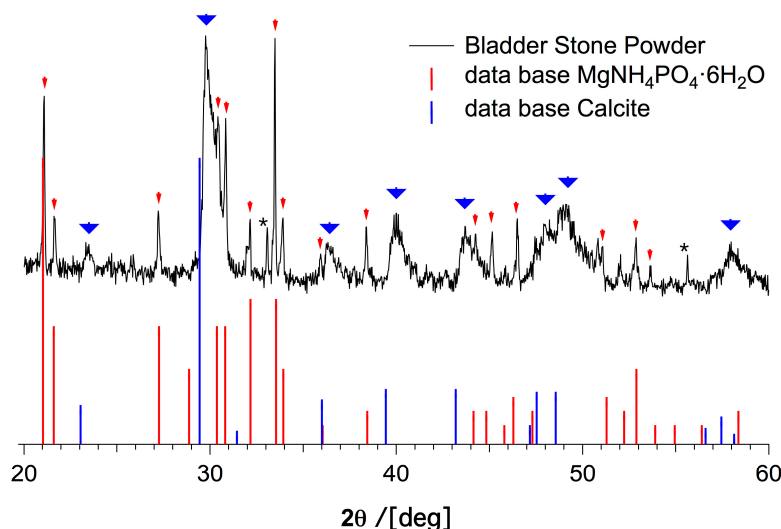


Figure 3. Top trace: X-ray diffractogram of the powdered urinary stone. Bottom lines: literature diffractograms for magnesium ammonium phosphate (struvite, $\text{MgNH}_4\text{PO}_4 \cdot 6\text{H}_2\text{O}$) (red) and calcite (blue). The asterisks (*) label reflections that cannot be unambiguously assigned.

It is important to note that the rather low signal-to-noise (S/N) ratio is not due to fast data acquisition, but rather due to a low amount of crystallinity in the sample. The reflections from struvite are marked with red arrows, and the broad reflections that may be assigned to calcite are marked with thick blue arrows (Figure 3). Interestingly, the pattern for the calcite phase is shifted by $\sim 0.3^\circ$ to larger angles as compared with the calcite database diffractogram. Given the internal struvite reference, the shift has to be considered real, although a constant shift in all reflections is surprising and usually due to a misalignment of the diffractometer. The shift of the reflections is not consistent with monohydrocalcite [44], which has a similar diffraction pattern as calcite, but with a shift to lower angles. Due to the low S/N ratio, despite a long acquisition time, and the broad reflections, we cannot unambiguously assign this reflection pattern to calcite. To our knowledge, such broad features have not been reported for calcite, which typically tends to exhibit narrow and intense reflections, but it may well be due to nano-calcite. Another possible explanation for this broadening is the accommodation of magnesium ions in the calcite lattice, which can cause significant broadening of the reflections [45,46]. Quantitatively, the observed shift in the (104) reflection of calcite without magnesium substitution ($2\theta = 29.429^\circ$) to $2\theta \approx 29.8^\circ$ (maximum of the reflection) gives a change in $d_{(104)}$ from 3.0326 Å (calcite) to ~ 3.0 Å, which is consistent with a Mg^{2+} content of ca. 10–20 mol % [45]. Owing to the low S/N ratio, it is difficult to extract the exact peak width in order to estimate the crystallite size via the Scherrer equation (assuming it is pure calcite) or, alternatively, to perform a Rietveld refinement for Mg-substituted calcite. In any case, the peak area of the broad reflections implies that this phase is more abundant than struvite.

Urinary stones of guinea pigs contain a small amount of organics in addition to the inorganic components [21]. We have used TGA in artificial air to determine the amount of organics, as well as the contents of struvite and calcium carbonate (Figure 4). The most pronounced mass loss can be assigned to the decomposition of the carbonate ions. Assuming that the observed loss of 30 % of relative weight, beginning at ca. 638 °C (Figure 4), is due to the calcination of calcium carbonate, yielding calcium oxide and carbon dioxide, we conclude that the urinary stone contains ~68 weight-% of CaCO₃ (see the Supplementary Materials). We note that in the light of the weak reflections in the XRD diffractogram (see above), the high carbonate content is actually surprising, and strongly suggests that a major part of the carbonates is in fact amorphous. Within this assumption, it follows that ca. 38 weight-% of the observed 49 weight-% remaining after reaching 820 °C is CaO (see the Supplementary Materials), indicating that ca. 10% are other (stable) inorganics. This level is consistent with the observed relative mass just before calcination (79%), which then is the sum of the relative masses of calcium carbonate and stable inorganics. The weight loss in between 112 and 162 °C (5%) may relate to decomposition/combustion of urea, which begins at 130 °C [47]. On the other hand, the decomposition of struvite, yielding magnesium hydrogenphosphate upon releasing ammonia and water, occurs in a single step between ~55 and 250 °C [48], and can hardly be separated from the decomposition/combustion of organics. Assuming that the ~10% of stable inorganics that remain after calcination of calcium carbonate, and that are not CaO, are magnesium hydrogenphosphate from struvite decomposition, the initial relative struvite content is ca. 20% (see the Supplementary Materials). This approach sums up to a total relative amount of inorganics of ca. 88%, suggesting that the stone contains ca. 12% organics, of which 5% may be urea. Based on this data, we cannot rule out the presence of amorphous magnesium carbonate or amorphous carbonated apatite, but since this TGA evaluation is consistent with quantitative EDS analyses (see below), these phases could constitute only minor fractions of the stone.

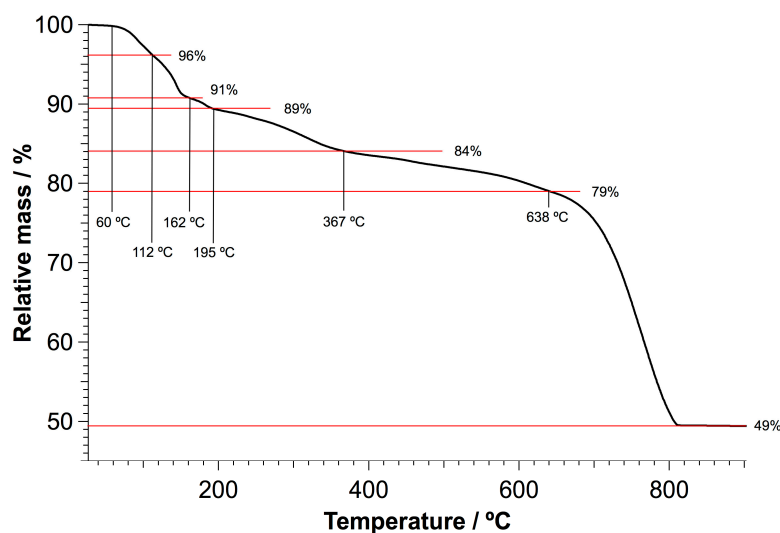


Figure 4. Thermal gravimetric analysis of the urinary stone of a guinea pig.

To study the compositional variation across the surface of the polished urinary stone, we recorded EDS maps. Figure 5 displays the EDS maps of the stone, in which clear and laminated ring patterns are observed not only for phosphorous but also for magnesium and oxygen. By comparison of the distribution of these elements with the SEM images, we conclude that struvite (MgNH₄PO₄·6H₂O) is concentrated within the denser regions of the laminated stone, which precipitates from urine at a pH of 9 in the presence of relatively small amounts of Mg²⁺ ions [49]. The other elements are rather evenly distributed throughout the area of the gently polished urinary stone, although calcium displays a similar pattern as the elements of struvite. Hence, the majority component according to TGA (calcium

carbonate) is present in both the dense and the loose regions and excluded from only some areas. Indeed, a close inspection of the EDS maps reveals that individual grains of struvite and calcium carbonate can be identified (white arrows in Figure 5). We speculate that the seed of the stone has been struvite (grain potentially located within the area indicated by a dashed yellow line in the SEM micrograph of Figure 5 considering the laminated pattern), which has served as a nucleus for further precipitation of calcium carbonate and inclusion or co-precipitation of other urinary constituents. The distribution of potassium, sodium, and chlorine is rather continuous, although some excluded areas are obvious, especially towards the outer perimeter. Lastly, silicon occurs randomly, likely being indicative of minor amounts of silica, taking the quantitative EDS data into account (see below, Table 1).

Figure 6 shows a magnified view on the porous region of the urinary stone with corresponding EDS mapping. Indeed, the calcium carbonate and struvite constituents of the stone are present as homogeneous and distinct phases in this part of the stone (white arrows mark micron-sized CaCO_3 particles in Figure 6). However, the EDS mapping also reveals regions that do not contain any of the traced elements (yellow arrow in Figure 6). We hypothesize that these regions are composed of urea. The compositional variations in the areas containing loosely packed inorganic particles appear to occur on relatively short length scales.

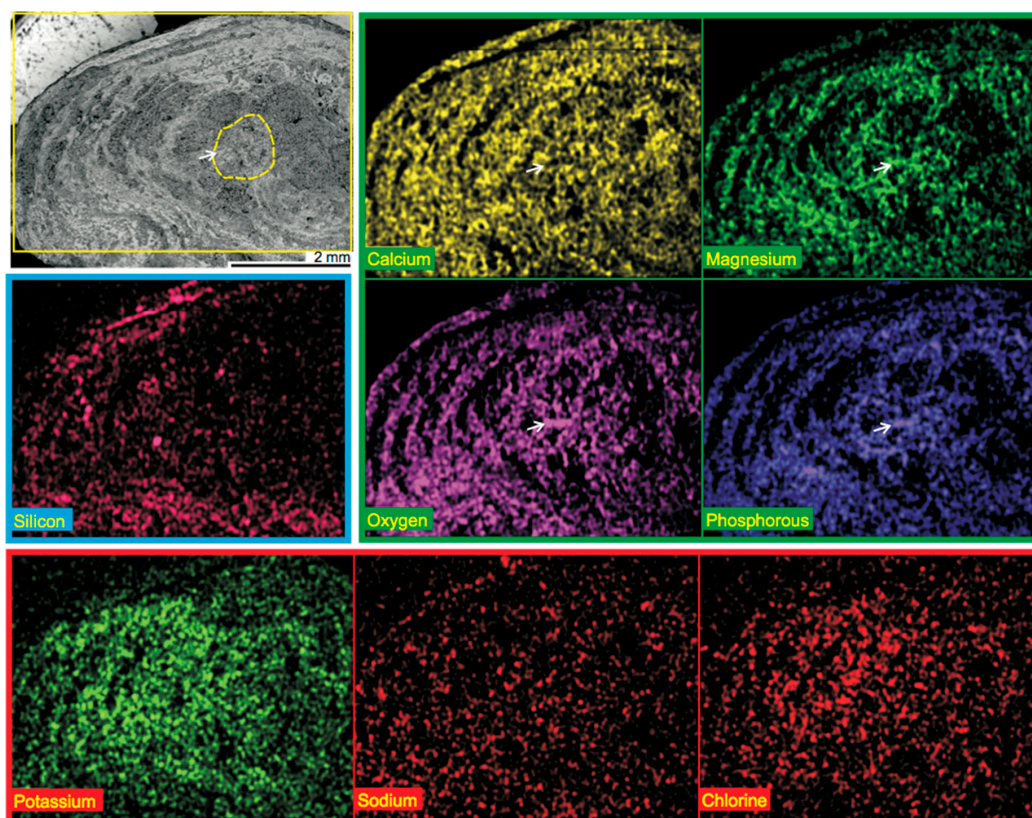


Figure 5. Energy-dispersive X-ray spectroscopy (EDS) maps of a cross-polished urinary stone from a guinea pig (overview, see Figure 6 for a magnified view). The top left image is the corresponding scanning electron micrograph, and the yellow frame indicates the area selected for EDS mapping. White arrows highlight an exemplified feature, where magnesium, oxygen, and phosphorous are abundant, but not calcium. This feature shows that although the contents of struvite and calcium carbonate are similarly distributed, larger individual grains can be identified. It may be speculated that struvite served as an initial seed within the yellow dashed area highlighted in the top left image. The EDS maps are grouped according to similar distributions within the urinary stone; calcium, magnesium, oxygen, and phosphorous (**green frame**); potassium, sodium, and chlorine (**red frame**); and silicon (**blue frame**).

The elemental composition of three spots of the urinary stone has been quantitatively determined by EDS, and is consistent with the composition determined from TGA (Table 1), which indicates ~68 weight-% of CaCO_3 , ~10 weight-% of struvite and other stable inorganics, ~5 weight-% of urea, and ca. 17 weight-% of other organics (see above). The first entry in Table 1 represents a larger spot that covers a loose and a dense area, the second one a smaller porous area, and the last entry a dense region (corresponding SEM images with detailed EDS results can be found in the Supplementary Materials, Figures S1–S3). It can be seen that the weight percentages of oxygen, carbon, calcium, potassium, and chlorine do not vary significantly within the distinct areas, whereas magnesium and phosphorous, both indicative of struvite, are somewhat more abundant in the dense region of the stone. Silicon, which indicates the location of the minor silica content, is somewhat increased within the porous region of the stone. However, given the rather inhomogeneous distribution of Si (see Figures 5 and 6), this may be a coincidental finding rather than a general compositional feature of the stone. Altogether, this additional EDS mapping indicates that significant structural variations can only occur on length scales smaller than ca. 200 μm .

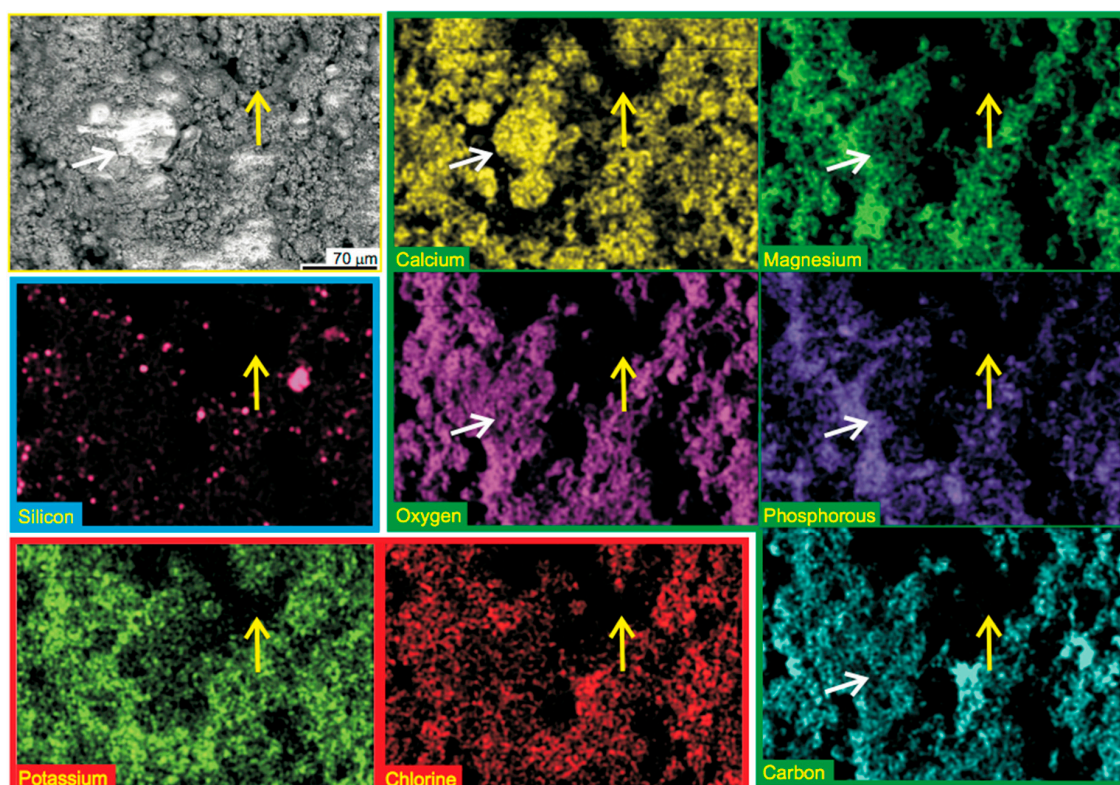


Figure 6. Energy-dispersive X-ray spectroscopy (EDS) maps of a cross-polished urinary stone of a guinea pig (magnified view of a porous region, see Figure 5 for an overview). The top left image is the corresponding scanning electron micrograph, and the yellow frame indicates the area selected for EDS mapping. White arrows highlight an exemplified feature in which calcium carbonate is abundant but magnesium and phosphorous is not. Yellow arrows mark a region where none of the investigated elements can be found to a significant extent. The EDS maps are grouped according to Figure 5; calcium, magnesium, oxygen, phosphorous, and carbon (green frame); potassium, and sodium (red frame); and silicon (blue frame).

Table 1. Elemental compositions estimated from electron-dispersive X-ray spectroscopy of three distinct regions in a cross-polished urinary stone of a guinea pig. The values represent weight percentages that have been normalized to 100%.

Element	Large Spot (weight-%)	Porous Region (weight-%)	Dense Region (weight-%)	Approx. Error (%)
Oxygen	48.5	49.5	50.2	6–8
Carbon	19.2	17.7	16.0	3–4
Calcium	20.7	18.6	16.9	0.5–0.7
Magnesium	5.1	6.4	7.2	0.3–0.4
Phosphorous	3.1	3.3	6.4	0.2–0.3
Potassium	2.2	2.6	2.1	0.1
Silicon	0.9	1.5	0.7	0.1
Chlorine	0.5	0.5	0.4	0

4. Conclusions

There is a variation in the components of the urinary stone of the guinea pig. The majority phase of the particular stone investigated here is calcium carbonate. The broad reflections for calcium (magnesium) carbonate and the fact that the stone contains 68 weight-% of calcium carbonate (based on TGA and EDS) indicate that a considerable fraction of the stone is ACC. ACC has to our knowledge not been documented for such urinary stones. The existence of ACC in the stone is consistent with the broad spectral features that can be assigned to carbonate vibrational modes in infrared spectroscopy (IR). It should be noted that ACC typically features very broad scattering in XRD. These are only evident for purely amorphous specimens and could not be observed for this stone that contains struvite and partially crystalline carbonates. The occurrence of ACC is generally also consistent with the presence of magnesium, which is known to kinetically stabilise ACC [40,50]. Transiently formed ACC [8] could be a precursor to monohydrocalcite (MHC) that can occur in such stones, whereas MHC might have transformed into Mg-calcite upon storage of the present stones [20]. The poor crystallinity of carbonates (Figure 3) might also indicate that they have formed via an amorphous precursor. While we cannot unambiguously prove the presence of ACC, further analyses based on TEM or polarized light microscopy would likely be inconclusive owing to the mixed composition of the stones. In any case, the present study shows that it could be important to further study if ACC is a common feature of urinary stones of guinea pigs. It should be emphasized that analyses [21] employing XRD cannot reveal the presence of ACC in samples with significant diffraction, and previously investigated stones may contain significant amounts of ACC. For example, the minute reflections due to calcium carbonate in the XRD analyses of the urinary stone of this study would have led to a dramatic underestimation of the calcium carbonate content, if the assessment would have been based on XRD alone. It is important to understand the occurrence of calcium carbonate, as it could potentially affect dietary recommendations. This can be a problem when the applied analytics is sensitive only for crystalline CaCO₃.

The stone displays successive laminated regions of dense and porous materials (growth rings), whereas crystalline struvite (MgNH₄PO₄·6H₂O) appears to be somewhat concentrated in the dense regions of the stone when considering the relative amounts of magnesium and phosphorous determined by means of EDS in the different regions (Table 1). The calcium carbonate is more evenly distributed than the magnesium salt within the urinary stone, which could be indicative of the fact that the precipitation of ACC occurred on already nucleated struvite particles. Further studies of the nucleation of urinary stones could be relevant to supporting this hypothesis. In any case, our results suggest that amorphous intermediates likely play a role in pathological precipitation of calcium carbonate. The kinetic stabilisation of the ACC against crystallisation in this particular case may be based on the presence of magnesium ions and organic constituents, and/or their combination [51].

Supplementary Materials: The following are available online at <http://www.mdpi.com/2075-163X/8/3/84/s1>, Figure S1: SEM micrograph with EDS mapping of a large area of the urinary stone of the Guinea Pig, Figure S2: SEM micrograph with EDS mapping of a smaller porous region of the urinary stone of the Guinea Pig, Figure S3: SEM micrograph with EDS mapping of a smaller dense region of the urinary stone of the Guinea Pig.

Acknowledgments: D.G. is a Research Fellow of the Zukunftscolleg of the University of Konstanz and is supported by the Fonds der Chemischen Industrie. N.H. thanks the Institute Excellence Center CODIRECT for funds. We thank Mia Winge for providing the urinary stone. This research did not receive any specific grant from funding agencies in the public, commercial, or not-for-profit sectors.

Author Contributions: D.G., M.O., and N.H. conceived and designed the experiments; D.G. and K.J. performed the experiments; D.G., K.J., and N.H. analyzed the data; D.G., K.J., and N.H. wrote the paper.

Conflicts of Interest: The authors declare no conflict of interest.

References

1. Lowenstam, H.A. *On Biomineralization*; Oxford University Press: New York, NY, USA, 1989.
2. Geyssant, J.; Huwald, E.; Strauch, D. *Calcium Carbonate: From the Cretaceous Period into the 21st Century*, Tegethoff, F.W., Ed.; English Ed.; Birkhäuser Verlag: Basel, Switzerland; Boston, MA, USA, 2001; ISBN 3-7643-6425-4.
3. Fratzl, P. Biomimetic materials research: What can we really learn from nature's structural materials? *J. R. Soc. Interface* **2007**, *4*, 637–642. [[CrossRef](#)] [[PubMed](#)]
4. Farhadi-Khouzani, M.; Schütz, C.; Durak, G.M.; Fornell, J.; Sort, J.; Salazar-Alvarez, G.; Bergström, L.; Gebauer, D. A CaCO₃/nanocellulose-based bioinspired nacre-like material. *J. Mater. Chem. A* **2017**, *5*, 16128–16133. [[CrossRef](#)]
5. Gebauer, D. Bio-Inspired Materials Science at Its Best-Flexible Mesocrystals of Calcite. *Angew. Chem. Int. Ed.* **2013**, *52*, 8208–8209. [[CrossRef](#)] [[PubMed](#)]
6. Natalio, F.; Corrales, T.P.; Panthöfer, M.; Schollmeyer, D.; Lieberwirth, I.; Müller, W.E.G.; Kappl, M.; Butt, H.-J.; Tremel, W. Flexible Minerals: Self-Assembled Calcite Spicules with Extreme Bending Strength. *Science* **2013**, *339*, 1298–1302. [[CrossRef](#)] [[PubMed](#)]
7. Gebauer, D.; Kellermeier, M.; Gale, J.D.; Bergström, L.; Cölfen, H. Pre-nucleation clusters as solute precursors in crystallisation. *Chem. Soc. Rev.* **2014**, *43*, 2348–2371. [[CrossRef](#)] [[PubMed](#)]
8. Addadi, L.; Raz, S.; Weiner, S. Taking advantage of disorder: Amorphous calcium carbonate and its roles in biomineralization. *Adv. Mater.* **2003**, *15*, 959–970. [[CrossRef](#)]
9. Weiner, S.; Mahamid, J.; Politi, Y.; Ma, Y.; Addadi, L. Overview of the amorphous precursor phase strategy in biomineralization. *Front. Mater. Sci. China* **2009**, *3*, 104–108. [[CrossRef](#)]
10. Cartwright, J.H. E.; Checa, A.G.; Gale, J.D.; Gebauer, D.; Sainz-Díaz, C.I. Calcium carbonate polyamorphism and its role in biomineralization: How many amorphous calcium carbonates are there? *Angew. Chem. Int. Ed.* **2012**, *51*, 11960–11970. [[CrossRef](#)] [[PubMed](#)]
11. Jahnen-Dechent, W.; Heiss, A.; Schäfer, C.; Ketteler, M. Fetuin—A regulation of calcified matrix metabolism. *Circ. Res.* **2011**, *108*, 1494–1509. [[CrossRef](#)] [[PubMed](#)]
12. Wesson, J.A.; Ward, M.D. Pathological Biomineralization of Kidney Stones. *Elements* **2007**, *3*, 415–421. [[CrossRef](#)]
13. Solomonov, I.; Weygand, M.J.; Kjaer, K.; Rapaport, H.; Leiserowitz, L. Trapping Crystal Nucleation of Cholesterol Monohydrate: Relevance to Pathological Crystallization. *Biophys. J.* **2005**, *88*, 1809–1817. [[CrossRef](#)] [[PubMed](#)]
14. Walton, R.C.; Kavanagh, J.P.; Heywood, B.R.; Rao, P.N. Calcium oxalates grown in human urine under different batch conditions. *J. Cryst. Growth* **2005**, *284*, 517–529. [[CrossRef](#)]
15. Long, J.R.; Shaw, W.J.; Stayton, P.S.; Drobny, G.P. Structure and Dynamics of Hydrated Statherin on Hydroxyapatite as Determined by Solid-State NMR. *Biochemistry* **2001**, *40*, 15451–15455. [[CrossRef](#)] [[PubMed](#)]
16. Jahnen-Dechent, W.; Schäfer, C.; Ketteler, M.; McKee, M. Mineral chaperones: A role for fetuin—A and osteopontin in the inhibition and regression of pathologic calcification. *J. Mol. Med.* **2008**, *86*, 379–389. [[CrossRef](#)] [[PubMed](#)]
17. Qiu, S.R.; Wierzbicki, A.; Orme, C.A.; Cody, A.M.; Hoyer, J.R.; Nancollas, G.H.; Zepeda, S.; De Yoreo, J.J. Molecular modulation of calcium oxalate crystallization by osteopontin and citrate. *Proc. Natl. Acad. Sci.* **2004**, *101*, 1811–1815. [[CrossRef](#)] [[PubMed](#)]

18. Luquet, G.; Marin, F. Biomineralisations in crustaceans: Storage strategies. *C. R. Palevol.* **2004**, *3*, 515–534. [[CrossRef](#)]
19. Reeder, R.J.; Tang, Y.; Schmidt, M.P.; Kubista, L.M.; Cowan, D.F.; Phillips, B.L. Characterization of Structure in Biogenic Amorphous Calcium Carbonate: Pair Distribution Function and Nuclear Magnetic Resonance Studies of Lobster Gastrolith. *Cryst. Growth Des.* **2013**, *13*, 1905–1914. [[CrossRef](#)]
20. Skinner, H.C.W.; Osbaldiston, G.W.; Wilner, A.N. Monohydrocalcite in a Guinea Pig bladder stone, a novel occurrence. *Am. Mineral.* **1977**, *62*, 273–277.
21. Hawkins, M.G.; Ruby, A.L.; Drazenovich, T.L.; Westropp, J.L. Composition and characteristics of urinary calculi from guinea pigs. *J. Am. Vet. Med. Assoc.* **2009**, *234*, 214–220. [[CrossRef](#)] [[PubMed](#)]
22. Hu, Q.; Nielsen, M.H.; Freeman, C.L.; Hamm, L.M.; Tao, J.; Lee, J.R.I.; Han, T.Y.J.; Becker, U.; Harding, J.H.; Dove, P.M.; De Yoreo, J.J. The thermodynamics of calcite nucleation at organic interfaces: Classical vs. non-classical pathways. *Faraday Discuss.* **2012**, *159*, 509–523. [[CrossRef](#)]
23. Nielsen, M.H.; Aloni, S.; De Yoreo, J.J. In situ TEM imaging of CaCO₃ nucleation reveals coexistence of direct and indirect pathways. *Science* **2014**, *345*, 1158–1162. [[CrossRef](#)] [[PubMed](#)]
24. Andreassen, J.-P.; Beck, R.; Nergaard, M. Biomimetic type morphologies of calcium carbonate grown in absence of additives. *Faraday Discuss.* **2012**, *159*, 247–261. [[CrossRef](#)]
25. Raiteri, P.; Gale, J.D. Water is the key to nonclassical nucleation of amorphous calcium carbonate. *J. Am. Chem. Soc.* **2010**, *132*, 17623–17634. [[CrossRef](#)] [[PubMed](#)]
26. Nassif, N.; Pinna, N.; Gehrke, N.; Antonietti, M.; Jäger, C.; Cölfen, H. Amorphous layer around aragonite platelets in nacre. *Proc. Natl. Acad. Sci.* **2005**, *102*, 12653–12655. [[CrossRef](#)] [[PubMed](#)]
27. Bazin, D.; Daudon, M.; Combes, C.; Rey, C. Characterization and Some Physicochemical Aspects of Pathological Microcalcifications. *Chem. Rev.* **2012**, *112*, 5092–5120. [[CrossRef](#)] [[PubMed](#)]
28. Kellermeier, M.; Gebauer, D.; Melero-García, E.; Drechsler, M.; Talmon, Y.; Kienle, L.; Cölfen, H.; García-Ruiz, J.M.; Kunz, W. Colloidal stabilization of calcium carbonate prenucleation clusters with silica. *Adv. Funct. Mater.* **2012**, *22*, 4301–4311. [[CrossRef](#)]
29. Gebauer, D.; Cölfen, H. Prenucleation clusters and non-classical nucleation. *Nano. Today* **2011**, *6*, 564–584. [[CrossRef](#)]
30. Bichler, K.-H.; Eipper, E.; Naber, K.; Braun, V.; Zimmermann, R.; Lahme, S. Urinary infection stones. *Int. J. Antimicrob. Agents* **2002**, *19*, 488–498. [[CrossRef](#)]
31. McLean, R.J.C.; Nickel, J.C.; Cheng, K.-J.; Costerton, J.W.; Banwell, J.G. The Ecology and Pathogenicity of Urease-Producing Bacteria in the Urinary Tract. *CRC Crit. Rev. Microbiol.* **1988**, *16*, 37–79. [[CrossRef](#)] [[PubMed](#)]
32. Peng, X.; Griffith, J.W.; Lang, C.M. Cystitis, urolithiasis and cystic calculi in ageing guineapigs. *Lab. Anim.* **1990**, *24*, 159–163. [[CrossRef](#)] [[PubMed](#)]
33. Stefov, V.; Šoptrajanov, B.; Kuzmanovski, I.; Lutz, H.D.; Engelen, B. Infrared and Raman spectra of magnesium ammonium phosphate hexahydrate (struvite) and its isomorphous analogues. III. Spectra of protiated and partially deuterated magnesium ammonium phosphate hexahydrate. *J. Mol. Struct.* **2005**, *752*, 60–67. [[CrossRef](#)]
34. Gebauer, D.; Gunawidjaja, P.N.; Ko, J.Y.P.; Bacsik, Z.; Aziz, B.; Liu, L.J.; Hu, Y.F.; Bergström, L.; Tai, C.W.; Sham, T.K.; Edén, M.; Hedin, N. Proto-calcite and proto-vaterite in amorphous calcium carbonates. *Angew. Chem. Int. Ed.* **2010**, *49*, 8889–8891. [[CrossRef](#)] [[PubMed](#)]
35. Brečević, L.; Nielsen, A.E. Solubility of amorphous calcium carbonate. *J. Cryst. Growth* **1989**, *98*, 504–510. [[CrossRef](#)]
36. Aizenberg, J.; Lambert, G.; Addadi, L.; Weiner, S. Stabilization of amorphous calcium carbonate by specialized macromolecules in biological and synthetic precipitates. *Adv. Mater.* **1996**, *8*, 222–226. [[CrossRef](#)]
37. Günther, C.; Becker, A.; Wolf, G.; Epple, M. In vitro synthesis and structural characterization of amorphous calcium carbonate. *Z. Für Anorg. Allg. Chem.* **2005**, *631*, 2830–2835. [[CrossRef](#)]
38. Kojima, Y.; Kawanobe, A.; Yasue, T.; Arai, Y. Synthesis of amorphous calcium carbonate and its crystallization. *J. Ceram. Soc. Jpn.* **1993**, *101*, 1145–1152. [[CrossRef](#)]
39. Lam, R.S.K.; Charnock, J.M.; Lennie, A.; Meldrum, F.C. Synthesis-dependant structural variations in amorphous calcium carbonate. *CrystEngComm* **2007**, *9*, 1226–1236. [[CrossRef](#)]
40. Lose, E.; Wilson, R.M.; Seshadri, R.; Meldrum, F.C. The role of magnesium in stabilising amorphous calcium carbonate and controlling calcite morphologies. *J. Cryst. Growth* **2003**, *254*, 206–218. [[CrossRef](#)]

41. Vagenas, N.; Gatsouli, A.; Kontoyannis, C.G. Quantitative analysis of synthetic calcium carbonate polymorphs using FT-IR spectroscopy. *Talanta* **2003**, *59*, 831–836. [[CrossRef](#)]
42. Gueta, R.; Natan, A.; Addadi, L.; Weiner, S.; Refson, K.; Kronik, L. Local atomic order and infrared spectra of biogenic calcite. *Angew. Chem. Int. Ed.* **2007**, *46*, 291–294. [[CrossRef](#)] [[PubMed](#)]
43. Coe, F.L. Kidney stone disease. *J. Clin. Invest.* **2005**, *115*, 2598–2608. [[CrossRef](#)] [[PubMed](#)]
44. Effenberger, H. Kristallstruktur und Infrarot-Absorptionsspektrum von synthetischem Monohydrocalcit, $\text{CaCO}_3 \cdot \text{H}_2\text{O}$. *Monatshefte Für Chem.* **1981**, *112*, 899–909. [[CrossRef](#)]
45. Goldschmidt, J.R.; Graf, D.L. Relation between lattice constants and composition of the Ca-Mg carbonates. *Am. Mineral.* **1958**, *43*, 84–101.
46. Tompa, É.; Nyirő-Kósa, I.; Rostási, Á.; Cserny, T.; Pósfai, M. Distribution and composition of Mg-calcite and dolomite in the water and sediments of Lake Balaton. *Cent. Eur. Geol.* **2014**, *57*, 113–136. [[CrossRef](#)]
47. Schaber, P.M.; Colson, J.; Higgins, S.; Thielen, D.; Anspach, B.; Brauer, J. Thermal decomposition (pyrolysis) of urea in an open reaction vessel. *Thermochim. Acta* **2004**, *424*, 131–142. [[CrossRef](#)]
48. Bhuiyan, M.I.H.; Mavinic, D.S.; Koch, F.A. Thermal decomposition of struvite and its phase transition. *Chemosphere* **2008**, *70*, 1347–1356. [[CrossRef](#)] [[PubMed](#)]
49. Ronteltap, M.; Maurer, M.; Gujer, W. The behaviour of pharmaceuticals and heavy metals during struvite precipitation in urine. *Water Res.* **2007**, *41*, 1859–1868. [[CrossRef](#)] [[PubMed](#)]
50. Politi, Y.; Batchelor, D.R.; Zaslansky, P.; Chmelka, B.F.; Weaver, J.C.; Sagi, I.; Weiner, S.; Addadi, L. Role of magnesium ion in the stabilization of biogenic amorphous calcium carbonate: A structure–function investigation. *Chem. Mater.* **2010**, *22*, 161–166. [[CrossRef](#)]
51. Wolf, S.L.P.; Jähme, K.; Gebauer, D. Synergy of Mg^{2+} and poly(aspartic acid) in additive-controlled calcium carbonate precipitation. *CrystEngComm* **2015**, *17*, 6857–6862. [[CrossRef](#)]



© 2018 by the authors. Licensee MDPI, Basel, Switzerland. This article is an open access article distributed under the terms and conditions of the Creative Commons Attribution (CC BY) license (<http://creativecommons.org/licenses/by/4.0/>).